SIMULATION OF THREE-DIMENSIONAL INCOMPRESSIBLE CAVITY FLOWS

H Yao, R K Cooper, and S Raghunathan
School of Aeronautical Engineering
The Queen's University of Belfast, Belfast BT7 1NN, UK

Keywords: *three-dimensional cavity, incompressible flow, Navier-Stokes equations*

Abstract

This paper investigates incompressible, unsteady flow over 3-dimensional cavities. Previous research in incompressible flow with cavities has included flow inside and over a 2-dimensional cavity, and flow inside a 3-dimensional cavity, driven by a moving lid. The present research is focused on incompressible flow over 3-dimensional open shallow cavities. This involves the complex interaction between the external flow and the re-circulating flow inside the cavity. A computational fluid dynamics approach, based on the unsteady Navier-Stokes equations, is used in the study.

Typical results of computation with the Reynolds number equaling 3000 are presented. Unsteady vortical structures and shear-layer oscillations are observed within and around the cavities.

1 Introduction

Several aerodynamic configurations include cavities as an integral part of design, manufacture, and performance. Flow over a cavity is often characterized by unsteady velocity and density, and furthermore by unsteady pressure fluctuation [1]. Surface defects such as cavities increase the skin friction of a surface (e.g. wing) and affect the operation cost. Development of control techniques to reduce the drag and to alleviate the pressure fluctuation produced by a cavity requires a fundamental understanding of aerodynamics of complex flow over such a geometry [2]. Cavity flow is also a topic relevant to aero-acoustics and transition studies.

During the past years, both experimental and computational studies have been conducted into the cavity flow structures. However, these studies were mainly focused on compressible, particularly supersonic flows [3][4]. Although there have been some studies considering incompressible cavity flow, these were mainly focused on flow inside or around 2-dimensional cavity (e.g. [5]-[9]), or flow *inside* 3-dimesional cavity known as lid-driven cavity (e.g. [10]-[12]). Lid-driven cavity flow does not take into consideration the interaction between the external flow and the re-circulating flow inside the cavity. This interaction can be observed for the flows passing over the cavity. A shear layer forms between the external flow and re-circulating internal flow. This shear layer is inherently unstable, which may flow over or bridge a cavity (i.e. open cavity), or deflect inwards with a possible impingement on the floor (i.e. closed cavity). Open-cavity flow fields are remarkably complicated, with the internal and external regions that are coupled via self-sustained shear layer oscillations. In order to understand this complex flow structure, numerical studies were performed on 3-dimensional cavities, assuming a rectangular geometry.

Open cavities are commonly classified into 'shallow' or 'deep', according to the depth-to-length (D/L) ratio. Following [13], cavities with D/L less than one are described as 'shallow cavities', while cavities with D/L greater than one are considered to be 'deep cavities'. The present research is an extension of the authors' previous work [14] from 3-dimensional *deep* open cavity to 3-dimensional *shallow* open cavity. Flow over shallow, open

cavities exhibits constant amplitude shear-layer oscillations. A CFD approach is used in this study.

2 Methodology

The flows to be modelled are assumed to be 3-dimensional, incompressible and unsteady. In addition, they are also assumed to be laminar.

2.1 Governing equations

The governing equations are based on the 3-dimensional, unsteady, incompressible Navier-Stokes equations. In Cartesian coordinates, these equations can be written, in a dimensionless form, as

$$\nabla \cdot \vec{u} = 0 \qquad (1)$$

$$\frac{\partial \vec{u}}{\partial t} + \vec{u} \cdot \nabla \vec{u} = -\nabla p + \frac{1}{R_e} \nabla^2 \vec{u} \qquad (2)$$

Where, based on reference length L and velocity U_∞,

$\vec{u} = \vec{u}(\vec{x}, t)$ is the dimensionless velocity vector, with $\vec{x}$ and t representing the dimensionless vector of coordinates and dimensionless time, respectively;

$p = p(\vec{x}, t)$ is the dimensionless pressure;

$R_e = U_\infty L / \nu$ is the Reynolds number, with U_∞ being the free stream velocity, L being the length of the cavity and ν being the kinematic viscosity.

One of the primary difficulties for solving Equations (1) and (2) is to couple changes in the velocity field with changes in the pressure field while satisfying the continuity condition, Equation (1). To overcome this difficulty, a pressure Poisson equation has been established to obtain the pressure field [15]. This equation is jointly solved with Equation (2) to obtain the solutions to both the pressure and velocity. The obtained velocity solution can satisfy the required continuity condition. In this method, the velocity and pressure are indirectly coupled.

The pressure Poisson equation can be obtained by taking the divergence of Equation (2). This gives

$$\nabla^2 p = \nabla \cdot (\frac{1}{\mathrm{Re}} \nabla \vec{u} - \vec{u} \cdot \nabla \vec{u}) - \nabla \cdot (\frac{\partial \vec{u}}{\partial t}) \qquad (3)$$

Equations (1)-(3) constitute the mathematical model used in the computation.

2.2 Numerical method

The numerical scheme used was the second-order implicit Crank-Nicolson finite difference scheme, with second-order accuracy in both time and space. At each time step the computation involves the solution of a linear algebraic system with a tri-diagonal matrix. This can be efficiently solved using the alternating direction implicit (ADI) method, which is the method employed in present computation.

Fig. 1 shows the geometric configuration of the rectangular cavity, with a length L, width W and depth D, used for computation. It is assumed that the flow is symmetric with respect to the longitudinal center plane, therefore only a half span of the cavity is chosen to be the computational domain.

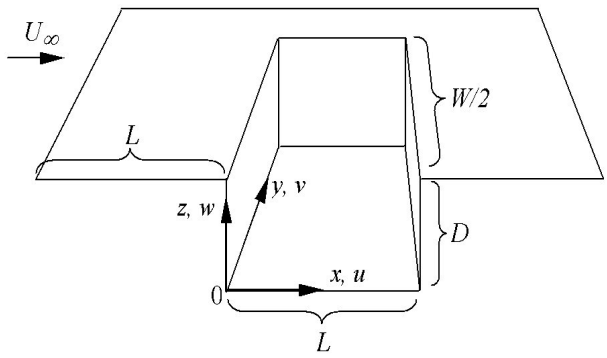

Fig. 1 Geometry of the rectangular half-span cavity used for computation

A uniform in-flow U_∞ is assumed so that a thin laminar boundary layer is developed at the lip of the cavity. The out-flow is specified by zero'th-order extrapolation from the computation zone. The entire flow field above the cavity is initialized with the in-flow condition, and the flow field within the cavity is initialized to zero. The initial pressure is set to its free stream value. No-slip boundary condition is used on solid surfaces, where the pressure is obtained by an extrapolation of the interior point values of the pressure in the direction normal to the wall. At the upstream boundary, the *y* and *z* component velocities, *v* and *w*, are assumed to be zero. The flow variables at the downstream boundary are also obtained based on zero'th-order extrapolation.

Three-dimensional Cartesian non-uniform Cartesian grids are generated with clustering of nodes near walls and in the shear layer region. These clustered nodes account for greater gradients in velocity and pressure in these regions.

2.3 Code Validation

The code has been examined using both analytical and numerical examples given in [11]; the numerical examples used for the validation include both 2-dimensional and 3-dimensional cavity flow fields. A detailed description of these validation studies can be found in [14]. Both the analytical and numerical case studies have validated the code.

3 Typical Results and Discussion

This section describes the results of computation of incompressible flow over 3-dimensional rectangular open shallow cavities. In particular, two depth-to-length ratios are considered, which are $D/L = 0.5$ and $D/L = 0.25$, respectively; in both cases, the width-to-length ratio is $W/L = 3$. The following presents the results obtained with the Reynolds number $R_e = 3000$, chosen based on the length of the cavity.

3.1 Case 1

In case 1, the cavity with a depth-to-length ratio $D/L = 0.5$ is simulated. Fig. 2 shows the cavity flow fields of the longitudinal (i.e. *x*) direction, at the $y = 0$ (i.e. symmetry) plane and at the dimensionless time $t = 204$. Specifically, Fig. 2(a) indicates the velocity vectors; Fig. 2(b) is a blow-up of the velocity vectors inside the cavity; and Fig. 2(c) shows the instantaneous vorticity contours. Fig. 2(b) shows the primary vortex, and a secondary vortex upstream. In addition, a tertiary vortex is formed in the front of the cavity below the free shear layer. Since the tertiary and the primary vortices rotate in a clockwise direction, a saddle point exists in the flow field between their cores. These vortex phenomena have also been found in 2-dimensional open shallow cavities [6]. Fig. 2(c) clearly shows the free shear layer oscillations above the cavity and in the downstream boundary layer.

Away from the symmetry plane, Fig. 3 and Fig. 4 show the cavity flow fields of the *x* direction at the $y = 0.9$ and $y = 1.2$ planes, respectively, at $t = 204$. Compared to Fig. 2(b), in Fig. 3(b) (i.e. the $y = 0.9$ plane) the primary vortex becomes larger, the secondary and tertiary vortices become weaker, and a vortex is found at the lower corner downstream. It seems that the tertiary vortex is merged into the primary vortex in Fig. 3(b). However, in Fig. 4(a), i.e. the $y = 1.2$ plane, a similar flow structure is found to that for the symmetry plane. These clearly indicate the 3-dimensional nature of the flow field. The vorticity contours included in these figures show the shear layer oscillations at the corresponding planes, respectively. For these three planes, the strongest oscillation is seen at the $y = 0.9$ plane due to the largest primary vortex.

Fig. 5 to Fig. 7 show the cross flow velocity vectors and vorticity contours of the lateral planes at $x = 0.5$, $x = 0.7$ and $x = 1.4$, respectively (relative to the front wall of the cavity). Fig. 5 indicates that the cross flow is weak in the front end of the cavity, but with visible shear layer oscillation in the lateral

direction. In Fig. 6, i.e. the $x = 0.7$ plane, the longitudinal vortices are found at the top and floor of the cavity. These vortices, interacting with the changing primary vortex along the lateral direction, cause the oscillation in the shear layer at the lateral direction. These oscillations are propagated downstream. This is evident in Fig. 7, corresponding to the cross flow at the $x = 1.4$ plane, which is aft of the cavity. The longitudinal vortices can be clearly seen; the vortices in the shear layer are stronger than at both of the $x = 0.5$ and $x = 0.7$ planes. Based on Fig. 2 to Fig. 7, it is not difficult to find that the investigated cavity flow field is unsteady.

3.2 Case 2

In case 2, the cavity with a depth-to-length ratio $D/L = 0.25$ is simulated. Fig. 8 shows the flow structure of the longitudinal direction at the $y = 0$ and $y = 1.0$ planes, respectively. As can be seen, the flow structures at these two planes are similar. In fact, this similarity is also found between the flow structures at other planes for which computation have also been performed (e.g. $y = 0.9$, $y = 1.2$ etc.). Thus, the size of the primary vortex, located downstream in the cavity, does not change significantly with the planes. This may explain why there is no significant shear layer oscillation being found in these flow fields. These are considerably different from the observations obtained earlier for the cavity with $D/L = 0.5$, in Case 1.

Fig. 9 shows the cross flow velocity vectors of the lateral direction at $x = 0.5$ and $x = 0.85$ planes (relative to the front wall of the cavity). At the $x = 0.5$ plane (Fig. 9(a)), the cross flow is so weak that it is difficult to be seen. A small longitudinal vortex is only found at the planes closer to the rear wall of the cavity, at the lower corner of the cavity (e.g. Fig. 9(b)).

4 Conclusions

This paper investigated the numerical simulation of incompressible flow over 3-dimensional open shallow rectangular cavities, with a Reynolds number of 3000, and a cavity geometry of $W/L = 3$, and $D/L = 0.5$ and $D/L = 0.25$, respectively. In the case with $D/L = 0.5$, the flow exhibits a 3-dimensional nature, and unsteady vortical structures and shear-layer oscillations are observed within and around the cavities. In the case with $D/L = 0.25$, it is found that the flow tends to be stable, and thus exhibits a 2-dimensional nature. Further studies are being undertaken for higher Reynolds numbers.

References

[1] Rockwell D and Naudascher E. Review-self-sustaining oscillations of flow past cavities. *ASME Journal of Fluid Engineering*, Vol. 100, pp. 152-165, 1978.

[2] Suhs N E. Computions of three-dimensional cavity flow at subsonic and supersonic Mach numbers. *AIAA Paper 87-1208*, 1987.

[3] Baysal O, Srinivasan S and Stallings L Jr. Unsteady viscous calculations of supersonic flows past deep and shallow three-dimensional cavities. *AIAA Paper 88-0101*, 1988.

[4] Morgenstern A Jr and Chokani N. Hypersonic flow past cavities. *AIAA Journal*, Vol. 32, No. 12, pp. 2387-2393, 1994.

[5] Sinha S N, Gupta A K and Oberia M M. Laminar separating flow over backsteps and cavities part II: cavities. *AIAA Journal*, Vol. 20, No. 3, pp 370-375, 1982.

[6] Neary M D and Stsphanoff K D. Shear-layer-driven transition in a rectangular cavity. *Physics of Fluids*, Vol. 30, No. 10, pp 2936-2946, 1987.

[7] O'Brien V. Closed streamlines associated with channel flow over a cavity. *Physics of Fluids*, Vol. 15, No. 12, 1972.

[8] Wood W A. Multigrid approach to incompressible viscous cavity flow. *NASA TM-110262*, 1996.

[9] Pereira J C F and Sousa J M M. Experimental and numerical investigation of flow oscillations in a rectangular cavity. *ASME Journal of Fluid Engineering*, Vol. 117, pp 68-74, 1995.

[10] Koseff J R and Street R L. On end wall effects in a lid-driven cavity flow. *ASME Journal of Fluid Engineering*, Vol. 106, pp 385-389, 1984.

[11] Chiang T P, Hwang R R and Sheu W H. On end-wall corner vortices in a lid-driven cavity. *ASME Journal of Fluid Engineering*, Vol. 119, pp 201-204, 1997.

[12] Cortes A B and Miller J D. Numerical experiments with the lid-driven cavity flow problem. *Computer Fluids*, Vol. 23, pp 1005-1027, 1994.

[13] Sarohia V. Experimental investigations of oscillations in flows over shallow cavities. *AIAA Journal*, Vol. 15, No. 7, pp 984-991, 1977.

[14] Yao H, Cooper R K and Raghunathan S. Computation of incompressible flow over three-dimensional cavities. *Third International Conference on Advances in Fluid Mechanics* (AFM2000), Montreal, Canada, 2000.

[15] Rogers S E and Kwak D. Upwind difference scheme for the time-accurate incompressible Navier-Stokes equations. *AIAA Journal*, Vol. 28, pp. 253-262, 1990.

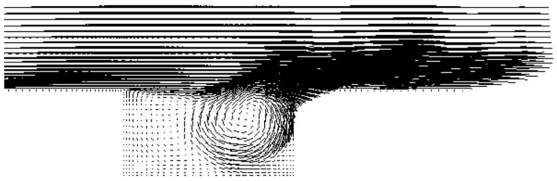

(a) Velocity vectors

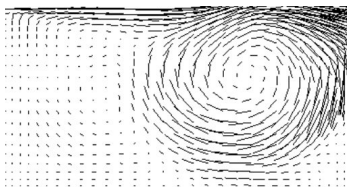

(b) Blow-up of (a) for the velocity vectors inside the cavity

(c) Vorticity contours of (a)

Fig. 2 Flow fields of *x* direction at $y = 0$ plane
Cavity geometry: $D/L = 0.5$, $W/L = 3$
$\mathrm{Re} = 3000$, $t = 204$

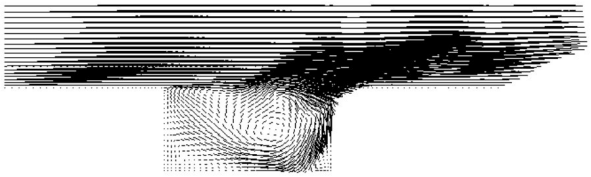

(a) Velocity vectors

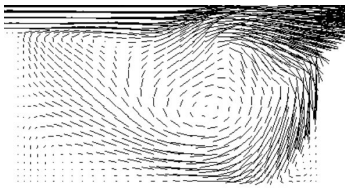

(b) Blow-up of (a) for the velocity vectors inside the cavity

(c) Vorticity contours of (a)

Fig. 3 Flow fields of *x* direction at $y = 0.9$ plane
Cavity geometry: $D/L = 0.5$, $W/L = 3$
$\mathrm{Re} = 3000$, $t = 204$

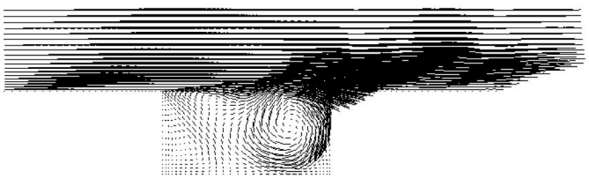

(a) Velocity vectors

(b) Vorticity contours of (a)

Fig. 4 Flow field of *x* direction at $y = 1.2$ plane
Cavity geometry: $D/L = 0.5$, $W/L = 3$
$\mathrm{Re} = 3000$, $t = 204$

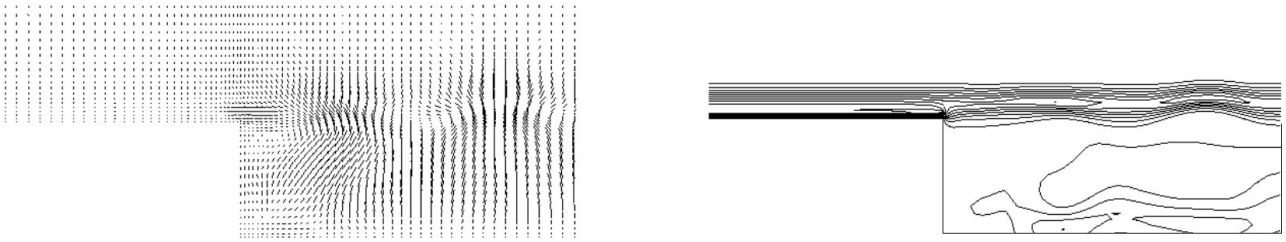

(a) Cross-flow velocity vectors

(b) Cross flow vorticity contours

Fig. 5 Cross-flow field at the lateral $x = 0.5$ plane (relative to the front wall of the cavity)
Cavity geometry: $D/L = 0.5$, $W/L = 3$
$\mathrm{Re} = 3000$, $t = 204$

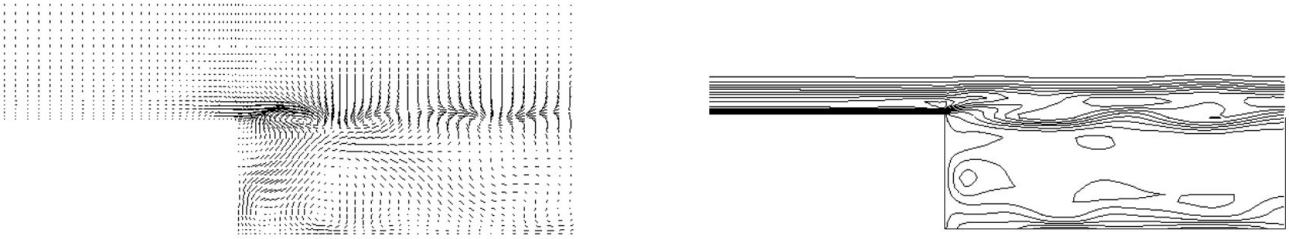

(a) Cross-flow velocity vectors

(b) Cross flow vorticity contours

Fig. 6 Cross-flow field at the lateral $x = 0.7$ plane (relative to the front wall of the cavity)
Cavity geometry: $D/L = 0.5$, $W/L = 3$
$\mathrm{Re} = 3000$, $t = 204$

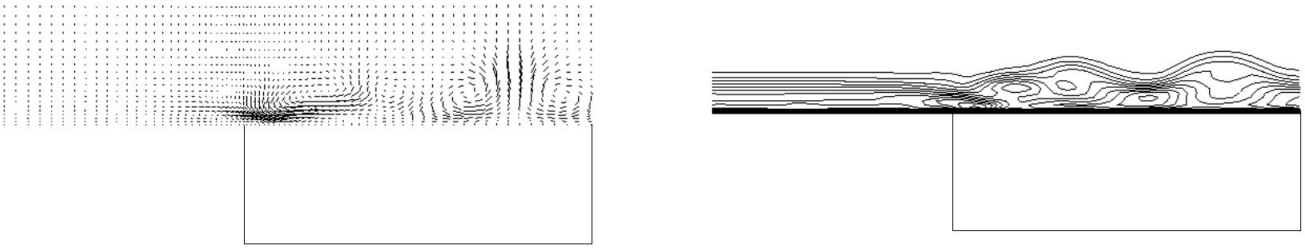

(a) Cross-flow velocity vectors

(b) Cross flow vorticity contours

Fig. 7 Cross-flow field at the lateral $x = 1.4$ plane (relative to the front wall of the cavity)
Cavity geometry: $D/L = 0.5$, $W/L = 3$
$\mathrm{Re} = 3000$, $t = 204$

(a) Velocity vectors at $y = 0$ plane

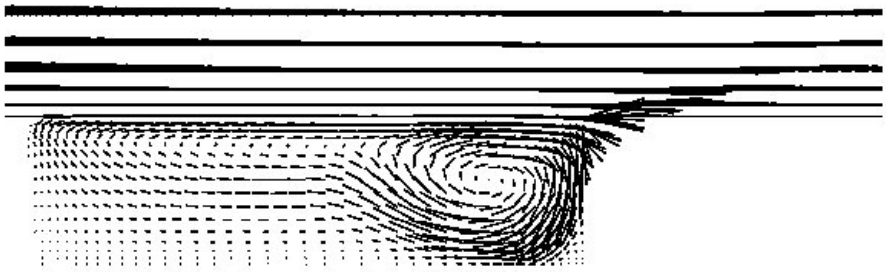

(b) Velocity vectors at $y = 1.0$

Fig. 8 Flow fields of *x* direction at different *y* planes
Cavity geometry: $D/L = 0.25$, $W/L = 3$, $\mathrm{Re} = 3000$

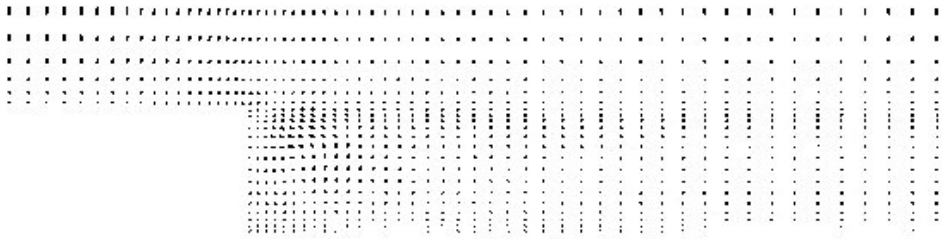

(a) Cross-flow velocity vectors at $x = 0.5$ plane

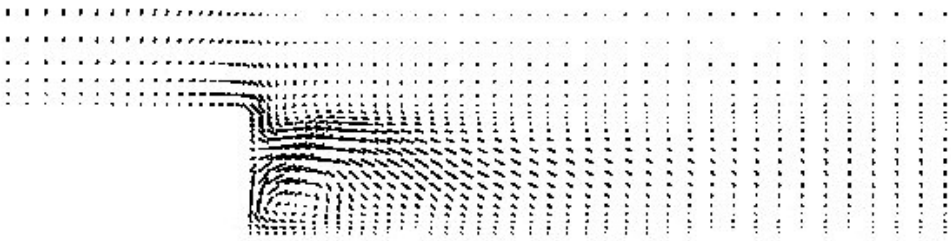

(b) Cross-flow velocity vectors at $x = 0.85$ plane

Fig. 9 Cross-flow fields at different lateral *x* planes (relative to the front wall of the cavity)
Cavity geometry: $D/L = 0.25$, $W/L = 3$, $\mathrm{Re} = 3000$